



Pyrite as prospective absorber material for monograin layer solar cell

Katriin Kristmann^a, Mare Altosaar^a, Jaan Raudoja^a, Jüri Krustok^{a,b}, Maris Pilvet^a,
Valdek Mikli^a, Maarja Grossberg^a, Mati Danilson^a, Taavi Raadik^{a,*}

^a Department of Materials and Environmental Technology, Tallinn University of Technology, Ehitajate Tee 5, 19086, Tallinn, Estonia

^b Division of Physics, Tallinn University of Technology, Ehitajate tee 5, 19086 Tallinn, Estonia

ABSTRACT

FeS₂ monograin powders as absorber materials in monograin layer solar cells were grown in the molten phase of two different flux materials - in liquid sulphur (S) and in potassium iodide (KI) at different temperatures - at 500 °C, 550 °C, 600 °C in S and at 740 °C in KI. The cooling temperature profiles were modified to preserve the pyrite phase of material until room temperature was reached. FeS₂ microcrystals, synthesized in sulphur and recrystallized in molten KI as flux, had cubic structure of pyrite phase with stoichiometric composition, confirmed by X-ray diffraction, Raman, and energy dispersive X-ray analyses, respectively. The grown FeS₂ crystals exhibited *n-type* conductivity determined by hot probe measurements. The powder crystals were fixed in monograin membranes for making heterostructures with *p-type* nickel oxide (NiO) buffer layer. Charge carrier concentrations 6.2×10^{16} and $2.5 \times 10^{17} \text{ cm}^{-3}$, were found from capacitance-voltage measurements using FeS₂/NiO heterostructures and FeS₂/Pt Schottky diodes, respectively.

1. Introduction

There is continuous search for cheap, earth abundant, environmentally friendly and nontoxic materials for solar cell absorber [1]. FeS₂ in the pyrite crystal structure is a promising candidate for solar cell absorber as it has suitable band gap of $E_g = 0.95 \text{ eV}$, effective light absorption coefficient ($\alpha > 10^5 \text{ cm}^{-1}$ for $h\nu > 1.3 \text{ eV}$), an adequate minority carrier diffusion length (100–1000 nm) and high electron mobility up to $360 \text{ cm}^2 \text{ V}^{-1} \text{ s}^{-1}$ at room temperature [2–5]. FeS₂ offers possibilities for electricity production at the lowest price compared with the other known solar cell materials. In a comparative study published in 2009 by Wadia et al. [6] involving different absorber materials, it was suggested that FeS₂ could be the cheapest material with the highest potential for electricity production, outweighing Si in every aspect. Some key topics that favour FeS₂ over Si were given in the ref. [6] as: extraction cost (\$1.70 per kg for Si vs \$0.03 per kg for Fe), the energy input for extraction (24 kWh kg⁻¹ for Si vs 2 kWh kg⁻¹ for Fe), and a low cost of the raw material per peak watt (0.039 ¢ per W for Si vs <0.000002 ¢ per W for FeS₂). Taking the earth abundance and extraction cost into consideration, it was speculated that a 4% efficient FeS₂ solar cell could produce the electricity at the same price that of a 19% efficient Si solar cell [6]. The theoretical calculated efficiency limit (the Shockley–Queisser limit) for pyrite solar cells is 25% [3]. FeS₂ has been explored for thin film solar cells, but after little progress the research has lately impeded. Since the first report of FeS₂ solar cells by A. Ennaoui

and H. Tributsch in 1984 [7] the FeS₂ solar cells have never shown power conversion efficiency (PCE) greater than 3% [3], despite high interest of scientists over three decades. Low PCE values are mainly the result of poor photovoltage, that never exceeds 0.3 V. Low PCE of FeS₂ is attributed to a high concentration of defects on the top surface of FeS₂ crystals, turning the crystals' surface *p-type*. FeS₂ thin films are commonly *p-type*, and they exhibit no photoelectrochemical response while single crystals are commonly *n-type* [2]. The origin of the unintentional *n-type* doping of pyrite FeS₂ is attributed to sulphur vacancies. In the review paper of K. Ellmer and C. Höffner [8] the authors concluded that FeS₂ is a stoichiometric compound having only slight deviations from the nominal sulphur-to-iron ratio of 2.0. The S deficiency on the surface of FeS₂ crystals is argued to be from 1 at% up to 13 at%, that may turn the bandgap of pyrite surface to zero and therefore highly conductive [2]. Volatile sulphur can easily leave from formed FeS₂ crystals' surfaces in these synthesis technologies where the escaping of sulfur is not held back, resulting in sulphur-poor composition of crystals' surface. M. Limpinsel et al. [9] showed that a hole-rich *p-type* surface layer was formed on the top of single crystals of FeS₂ and suggested that this *p-type* surface layer could possibly be eliminated by passivating surface states and subsurface defects. They showed that chemical surface treatments can substantially reduce the conductivity of the inversion layer.

This hole-rich inversion layer at the surface of pyrite crystals results in a leaky or small potential energy barrier [3,9]. Nesbitt et al. [10]

* Corresponding author.

E-mail address: taavi.raadik@taltech.ee (T. Raadik).

<https://doi.org/10.1016/j.tsf.2021.139068>

Received 18 June 2021; Received in revised form 17 December 2021; Accepted 17 December 2021

Available online 21 December 2021

0040-6090/© 2021 Elsevier B.V. All rights reserved.

studying iron surface states on fractured pyrite surface by XPS found two iron surface states Fe^{2+} and Fe^{3+} in addition to the iron bulk state. Iron ions' coordination is changed from octahedral before fracture to square pyramidal after fracture. The thin potential barrier could be caused by a symmetry reduction due to change in iron coordination number at the surface of the crystals. The symmetry reduction leads to Fe 3d states to lose their degeneracy and split into surface states that lie within the band gap with energies close to the valence band edge. When the Fermi level of the n -type bulk tends to equilibrate with surface states, it creates a strong upward band bending and an inversion layer [2]. As a result, donors near the surface rise above the Fermi level and are ionized. This creates a thin potential barrier for direct tunnelling of majority carriers. Both, the S-poor surface composition and the reduction of Fe – S coordination create near-surface deep ionized donor states at the bulk of material [2,3,11].

In order to control the formation of sulphur vacancies, it could be reasonable to synthesize pyrite in determined conditions in sulphur rich environment. Synthesis-growth method of semiconductor compounds in molten fluxes in evacuated quartz ampoules enables to grow semiconductor powder crystals (so called monograin powders) with uniform shape and composition. If the flux material is present in an amount sufficient to avoid the sintering of primary crystals, then it enables to raise repelling forces between solid particles, and individual single-crystalline powder particles can be formed and grown.

Aim of the present study was to develop a process to synthesize single phase FeS_2 microcrystals in the liquid phase of a flux material and apply these powders as absorber materials in monograin layer (MGL) solar cells. The MGL solar cell technology employs an absorber that is a monolayer of nearly unisize semiconductor powder crystals fixed in a thin layer of epoxy (or some other polymer) [12]. MGL solar cell has a superstrate solar cell structure: back contact / absorber / buffer / transparent conductive oxide. Before MGL preparation the powder crystals are coated with a thin layer of buffer material to create the p/n junction, after that each covered crystal is a tiny photovoltaic cell working in MGL solar cell in parallel connection. Therefore, the MGL technology has an advantage compared to other thin film technologies - it allows to separate (geographically) processes of absorber (powder) production from solar cell module formation. Current efficiency record of MGL solar cells is near 13% [13] and is achieved with copper-indium-gallium-selenide absorber. In the present study we tried to use liquid sulphur as flux but the removal of sulphur from formed FeS_2 crystals by vacuum sublimation turned out to harm the FeS_2 crystals' surfaces. Therefore, we used KI as flux for recrystallization and growth of bigger FeS_2 crystals. As the grown FeS_2 crystals showed n -type conductivity, we formed the p/n junction with a p -type buffer material (NiO).

2. Experimental description

FeS_2 microcrystals were synthesized and grown in a two-step process from binary compound FeS (Alpha Aesar, 3 N purity) and elemental S (3 N purity) in the liquid phase of S (first step) and recrystallized in KI (second step). Amount of S for synthesis was weighted considering that a part of it is consumed in the reaction to form FeS_2 and another part for the formation of liquid phase (flux) at the used synthesis temperatures, at 500, 550 and 600 °C. The temperatures were chosen according to the phase diagrams of iron-sulphur system [14,15], in order to stay in the pyrite phase region. The volume of liquid flux (V_L) (in both cases, S and KI) and the volume of solid FeS_2 (V_S) should be approximately equal as necessary for monograin growth [16]. The mixtures were sealed into evacuated quartz ampoules and heated in furnace for one week at temperatures stated before. After that, the process was stopped by quenching the ampoules in water. S as flux was tried to remove by vacuum sublimation, but this method resulted in powders showing Raman spectra with peaks of secondary phases. Therefore, leaching with KCN solution was used to release the FeS_2 powder crystals from the

excess of S. As the FeS_2 crystals released from S were too small for preparation of monograin membranes, the crystals synthesized at 600 °C were recrystallized in KI flux at 740 °C for one week to produce bigger crystals. The ampoule with recrystallized powder was slowly cooled in the furnace from 740 to 575 °C to ensure the phase transition of FeS_2 from a pyrrhotite mix (above 617 °C) to pyrite (below 617 °C) according to the phase diagram [14,17]. As per Yan-Hong Chen et al. [17] the iron-sulphur system has an abundance of different compositions above sulphur melting temperature at 118 °C [18]. These compositions include phases where the Fe:S molar ratio is 0.5–1 and depending on the system temperature, they consist of several different compositions, including pyrrhotite and Fe_{1-x}S mixtures. In an abundance of sulphur it is necessary to control the temperature limits to make sure to stay in the pyrite region of the phase diagram. The furnace was kept at 575 °C for 24 h, after that the ampoule was rapidly cooled by quenching in water. FeS_2 crystals were rinsed with deionized water to release them from solid KI-flux. The phase composition of the synthesized FeS_2 powders was studied by XRD and by Raman. XRD patterns were recorded on a Rigaku Ultima IV diffractometer with $\text{Cu K}\alpha$ radiation ($\lambda = 1.5406 \text{ \AA}$) operated at 40 kV and 40 mA in the 2θ range from 20 to 70° with a step of 0.002° and scanning rate of 5° per min. PDXL 2 software was used for the derivation of crystal structure information from the recorded XRD data. For Raman, the Horiba's LabRam HR800 spectrometer equipped with a multichannel CCD detection system in the backscattering configuration, was used. 532 nm laser line with spot size of 5 μm was used for excitation. The chemical composition of powders was determined by EDX using Bruker Esprit 1.8 system. The morphology of crystals was studied with the high-resolution scanning electron microscope (HR-SEM) Merlin operated with an accelerating voltage of 20 kV using a Röntec EDX XFlash 3001 detector. SEM equipment was combined with the EDX analysis equipment, which was used to analyse polished crystals surfaces and investigate the elemental distribution and compositional uniformity of different microcrystals. Conductivity type of crystals was determined by the hot probe method, where a sample crystal is placed between two indium probes. One probe is heated while the other stays at room temperature. The thermally excited free charge carriers move by diffusion from the hot probe to the cold probe. These majority carriers define the electrical potential sign in the multimeter. FeS_2 microcrystals exhibited n -type conductivity, determined by the hot probe method, so a new design of MGL solar cell was adopted with n -type absorber and p -type buffer layer. To prepare a FeS_2 MGL device the FeS_2 microcrystals were embedded in epoxy as a monolayer so that the upper surfaces of crystals remained uncovered. These monolayer membranes of pyrite were covered with a p -type NiO buffer layer. NiO was deposited by successive ionic layer adsorption and reaction (SILAR), recipe was adapted from Akaltun et al. [19]. This was followed by a soft heat treatment of 160 °C for 10 min to raise crystallinity of the NiO layer but not harm the epoxy membrane. To prepare FeS_2/Au and FeS_2/Pt Schottky diodes, the metals were deposited by vacuum evaporation and sputtering, respectively for Au and Pt. The hetero junctions were covered with a TCO layer and finished with a silver contact on top and graphite contacts on the pyrite side. Admittance spectra for FeS_2/NiO heterostructure and FeS_2/Pt Schottky diode were recorded by using a Wayne Kerr 6500B impedance analyser, charge carriers' density of pyrite was calculated using data from capacitance-voltage (C-V) measurements.

Changes in the chemical composition of crystals' surface after different growth and treatment methods were studied by X-ray photoelectron spectroscopy (XPS) using a Kratos Analytical Axis Ultra DLD spectrometer fitted with monochromatic Al $\text{K}\alpha$ X-ray source $\leq 0.5 \text{ eV}$ (Ag 3d_{5/2}) and achromatic Mg $\text{K}\alpha/\text{Al K}\alpha$ dual anode X-ray source $\leq 0.8 \text{ eV}$ (Ag 3d_{5/2}). The achromatic Mg $\text{K}\alpha$ X-ray source was used to collect secondary survey spectra in order to distinguish and separate the core level peaks and Auger peaks in XPS spectra. The relative atomic concentrations of the elements were determined from the appropriate integrated peak areas at the core level and the sensitivity factors provided

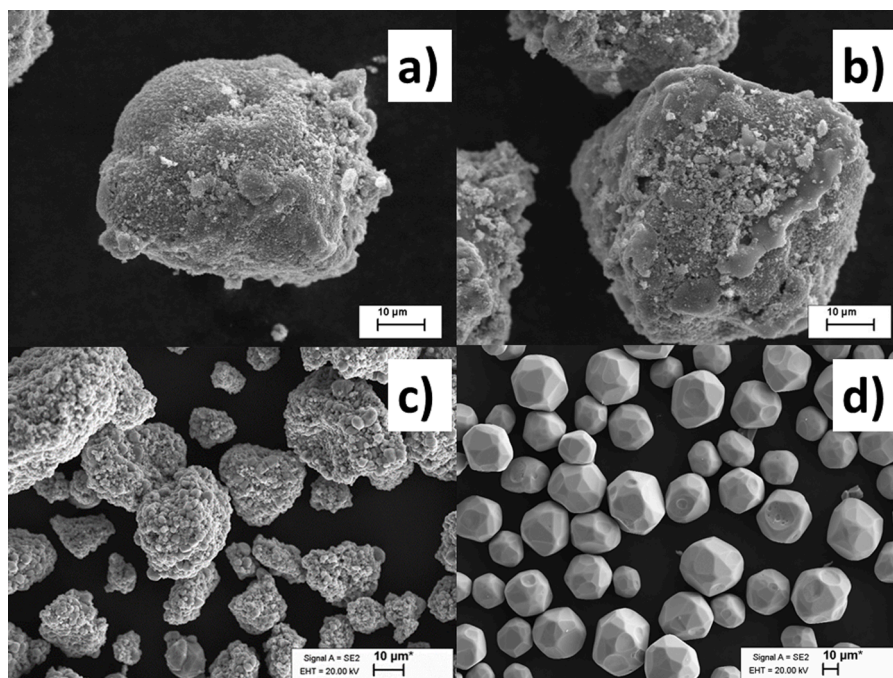


Fig. 1. SEM images of FeS₂ synthesized at a) 500 °C in S flux b) 550 °C in S flux c) 600 °C in S flux and d) FeS₂ crystals recrystallized at 740 °C in KI flux.

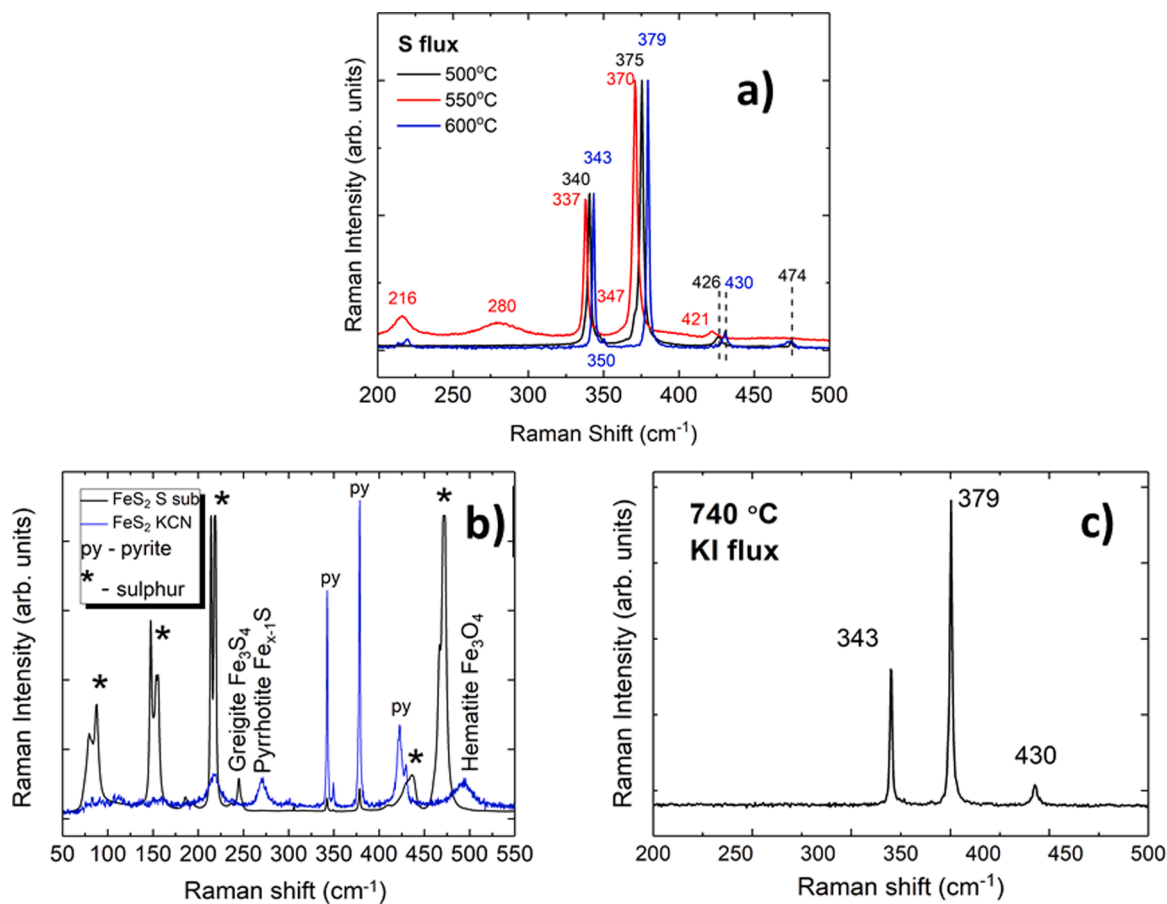


Fig. 2. a) Raman spectra of FeS₂ crystals synthesized at 500 °C, 550 °C and 600 °C in S flux. S was removed by vacuum sublimation and etching. b) Raman spectra of FeS₂ crystals synthesized at 550 °C in S flux. After vacuum sublimation (black line) and after sublimation and KCN etching (blue line). c) Raman spectrum of FeS₂ crystals recrystallized at 740 °C in KI flux.

by the original analysis Kratos Vision 2.2.10 software. The Shirley background subtraction was used to calculate relative atomic concentrations.

3. Results and discussion

3.1. Synthesis of FeS₂ crystals in S as a flux

In the first step FeS₂ was synthesized in the medium of liquid sulphur functioning as a flux. The surface morphology and shape of the synthesized crystals were characterized by SEM (see Fig. 1a, b, c). As it can be seen in Fig. 1a and Fig. 1b the FeS₂ crystals grown at 500 °C and 550 °C are not formed yet as single crystals, they consist of small particles sintered together.

Synthesis-growth that was performed at 600 °C (Fig. 1c), crystals have smoother surfaces, nevertheless the big conglomerates formed from smaller crystals can be seen. The average size of individual crystallites is around 1 µm. To grow bigger crystals there are two options, whether to increase time or temperature. As can be noticed, the growth at 600 °C resulted in slightly bigger crystals therefore the growth was performed at higher temperatures. Sulphur was found to be not the best flux material, because removing it via sublimation and/or KCN etching are time consuming, wasteful, and possibly harmful processes to the microcrystals' surface. However, KI seemed to be one of the best options to use as a flux material, because its melting point is 681 °C, it is a very stable compound and will not react with precursors [20], it is also water soluble.

3.2. Recrystallization of FeS₂ crystals in KI flux

KI has been used as flux in syntheses of different absorber materials for MGL solar cells: kesterites, CIGS and SnS [21–23]. The melting temperature of KI (681 °C) is lower than the decomposition temperature of FeS₂ into pyrrhotite and sulphur (744 °C) [15] and the presence of its liquid phase enhances the growth of individual grains of FeS₂ and inhibits the formation of agglomerates [5].

The FeS₂ powder synthesized in liquid sulphur at 600 °C (see the previous chapter) was recrystallized in KI as flux at 740 °C for one week. Formed crystals had a nice uniform shape and smooth surfaces (see Fig. 1d). Roughly half of the gained powder material was in the desired fraction size of around 50 µm.

3.3. Raman, EDX, XRD and hot probe results

Raman spectra of microcrystals synthesized in sulphur at different temperatures can be seen in Fig. 2a. Fig. 2b represents the Raman spectra of powders synthesized in S flux at 550 °C after the sublimation of sulphur under vacuum (black line) and after etching with a KCN solution (blue line). It is seen from Fig. 2b that when powders had only been treated under heated vacuum for sulphur sublimation, significant amount of sulphur remained amongst the material. Thus, it was decided to etch the microcrystals with KCN solution to dissolve and remove the surplus sulphur. After the etching process, there was significantly less elemental sulphur, but some of it was still evident. Sulphur poor phases such as greigite (Fe₃S₄) and pyrrhotite (Fe_{1-x}S), and an oxide phase haematite (Fe₂O₃) were also noticed from the Raman spectra. All powders on Fig. 2a have been synthesized at different temperatures in sulphur flux and treated with KCN etching to remove the excess sulphur. Microcrystals synthesized and recrystallized in KI are presented in Fig. 2c.

Raman peaks at 343, 350, 379 and a weak peak at 430 cm⁻¹ (Fig. 2a, b, c) are characteristic to the pyrite phase as reported in the literature [24,25]. Secondary phases present along with pyrite can be identified by Raman peaks: at 216 and 219 cm⁻¹ as characteristic to haematite (Fe₂O₃) [26] (in synthesis at 550 °C, Fig. 2a) and at 474 cm⁻¹ as characteristic to elemental sulphur [27] (in syntheses at 500 °C and 600 °C,

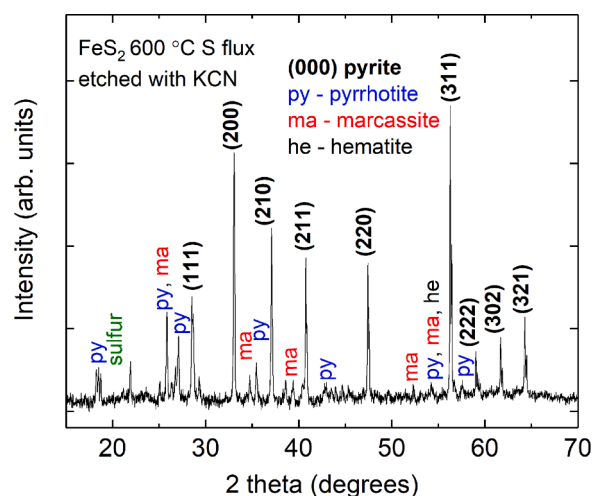


Fig. 3. XRD pattern of FeS₂ crystals synthesized in S flux, after vacuum sublimation and KCN etching.

Fig. 2a). Broad Raman band at 280 cm⁻¹ falls in the frequency region of amorphous or poorly crystallized metal–sulphur stretching mode and is attributed to FeS [28]. Deciding on the base of Raman analysis the purest pyrite phase is formed in recrystallisation of FeS₂ powder at 740 °C in KI followed by slow cooling to 575 °C (Fig. 2c). A slight variation in FeS₂ Raman peak positions can be seen in the Raman spectra of samples synthesized at 500 °C and 550 °C, that were post-annealed in vacuum for sulphur sublimation and etched with KCN solution. The shift in Raman peaks' positions could be related with removal of sulphur from the utmost surface layer of FeS₂ crystals causing the formation of S-deficient surface layer with variable composition. The shift in Raman peak positions via the formation of solid solutions has been reported to other compounds as well [29]. It is commonly related with the removal of sulphur from the utmost surface layer of FeS₂ crystals, which causes the formation of a variable S-deficient surface composition. The Fe–S bond length increases due to the strain–stress effect induced by decreasing sulphur concentration, which causes the wavenumbers to shift to lower values [29]. Reverse effect would shift the Raman peak position to higher values in the occurrence of sulphur rich composition. The shift in Raman peak positions from pyrite peaks at higher wavenumbers (synthesis at 600 °C, blue line) to lower wavenumbers (550 °C and 500 °C) is shown in Fig. 2a.

On the basis of Raman analysis, we can conclude that it is possible to

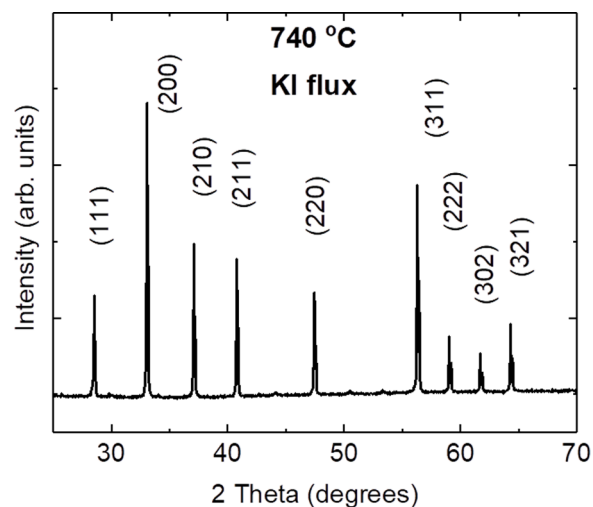


Fig. 4. XRD pattern of FeS₂ crystals recrystallized at 740 °C in KI flux.

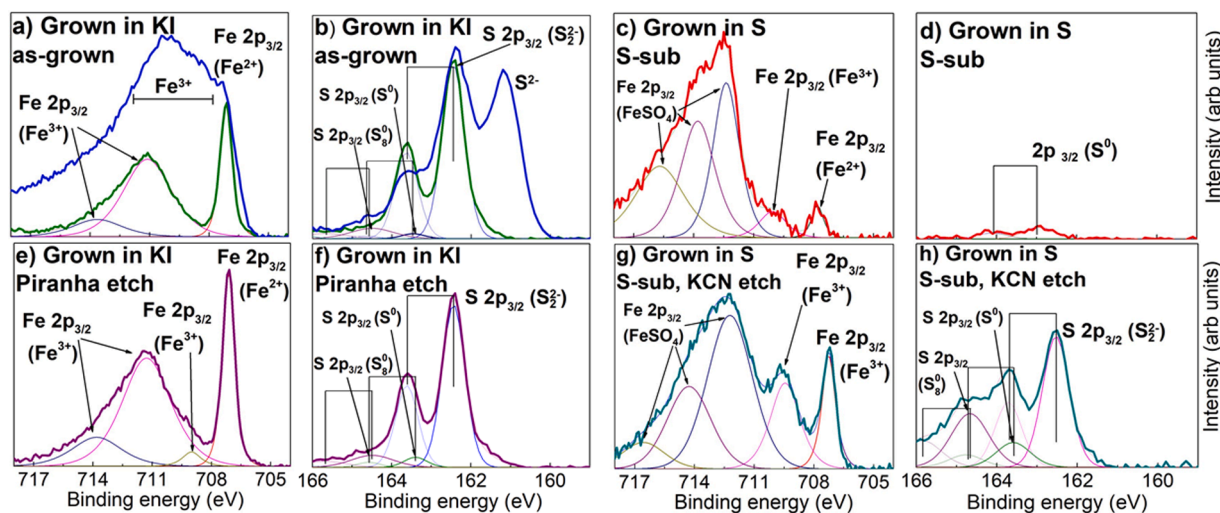


Fig. 5. High-resolution XPS core level spectra based on fitting results of Fe 2p and S 2p obtained from the surface of FeS₂ crystals grown in molten KI (Fig. 5a, b, e, f) and molten sulphur (Fig. 5c, d, g, h). XPS spectra were measured after dissolution of KI by water (Fig. 5a, b) marked as green line and after following etching with “Piranha” solution (Fig. 5e, f). Spectra of as-grown powders released from KI and sputtered with Ar⁺ ions for 60 s are also presented as blue lines in graphs Fig. 5a and Fig. 5b. XPS spectra from crystals grown in molten sulphur were recorded after removal of sulphur by vacuum sublimation (Fig. 5c, d) and after following chemical etching with KCN solution (Fig. 5c, d). Sulphur spectra on Fig. 5b, d, f, h exhibit 2p_{3/2} and 2p_{1/2} doublet signals with interval 1.2 eV, the doublets on graphs are marked by rectangular brackets, only the higher intensity component S 2p_{3/2} is shown for each doublet.

avoid the formation of unwanted iron sulphide phases if to proceed at higher temperatures, provide the conditions for phase transformation and quench the material quickly [15]. Synthesis route for phase pure pyrite was determined based on the Raman analysis. It is important to proceed at higher temperatures during the synthesis, provide the conditions for phase transformation into pyrite phase, and quench the material quickly for cooling to room temperature [15].

According to the EDX results, crystals grown at 500 °C have an iron rich composition of 39.21 at.% iron and 60.79 at.% sulphur. The composition shifts to more stoichiometric side with increasing growth temperature: crystals synthesized at 550 °C and 600 °C are closer to the stoichiometric composition of pyrite as 33.06 at.% Fe and 66.94 at.% S for 550 °C; 33.42 at.% Fe and 66.58 at.% S for 600 °C, respectively. Crystals recrystallized at 740 °C had composition of 33.77 at.% iron and 66.23 at.% sulphur. Even though EDX analyses showed almost stoichiometric compositions to the materials grown at 550 °C and 600 °C, there were still some additional phases and elemental sulphur that was confirmed by Raman.

The microcrystals were also analysed by XRD, the pattern can be seen in Fig. 3 and Fig. 4. XRD pattern of crystals that were synthesized in sulphur flux at 600 °C are seen on Fig. 3. These crystals had been etched with KCN solution to remove the S flux. Crystals that were recrystallized in liquid KI flux at 740 °C, where the flux had been removed by rinsing with water are seen on Fig. 4. It is evident from Fig. 3 that the powders include several additional crystalline phases such as marcasite and pyrrhotite in addition to pyrite. A possible haematite Fe₂O₃ peak was also observed in the XRD pattern. The quantity of different crystalline compositions can be related to the etching with KCN solution, which removed some of the sulphur, leaving a variable Fe_{1-x}S composition. It has been published by Chen et al. [17] that the iron-sulphur system has a multitude of phases in lower sulphur supply at different temperatures, that change the conditions for phase transition into pyrite and from pyrite into pyrrhotite. The XRD pattern of powders after recrystallization in KI at 740-755 °C shows that the additional phases are removed and transformed into pyrite phase. The resulting pure pyrite phase has lattice parameters $a = b = c = 5.4154 \text{ \AA}$, which confirms the cubic structure and agrees with the values reported in the literature [30–32]. Additionally, XRD supports Raman results that there are no secondary phases in the crystals recrystallized at 740 °C in KI flux.

As it is reported also in literature [11], all synthesized FeS₂ crystals

(at 500, 550, 600 and 740 °C) exhibited n-type conductivity according to the hot probe measurements.

3.4. XPS study of microcrystals

The XPS analysis was used to study the changes in the binding energies of constituent elements of FeS₂ crystals depending on different synthesis conditions and flux removal methods. XPS spectra of crystals grown in sulphur were recorded after removal of sulphur by vacuum sublimation and after additional chemical etching with KCN solution. FeS₂ crystals grown in molten KI flux were measured after dissolution of KI by water and after following etching with so called “Piranha” solution (H₂O₂ + H₂SO₄). Fig. 5a and Fig. 5b presents the XPS core level spectra of Fe 2p and S 2p before and after sputtering of the crystals surface for 60 s with Ar⁺ ions with the aim to remove the surface contamination seen in the XPS survey spectrum (not presented in this paper). But it can be noticed that Fe 2p and S 2p XPS spectra are strongly influenced by sputtering. After sputtering, all spectra in the iron region show a strong increase in signal in the area of Fe³⁺ species (shown as a horizontal line in Fig. 5a) while the signal of Fe²⁺ near 707 eV that belongs to pyrite [10] is much less intensive. In the energy region of sulphur XPS signals, the effect of sputtering is even stronger. In addition to the doublet signal of S 2p_{3/2} and S 2p_{1/2} (at 162.4 and 163.6 eV with the distance of 1.2 eV) that represents the emission of bulk S₂²⁻ [10,33,34] there emerges a peak at 161.3 eV characteristic to monosulfide S²⁻ surface state [10]. These afore described effects were present in all spectra of sputtered samples after each synthesis and treatment regime. The appearance of Fe³⁺ ionic states and S²⁻ monosulfide signals are similar to the phenomena characteristic to the pyrite surface mechanical fracturing described by Nesbitt et al. [10]. Due to the before described changes in XPS spectra accompanied with sputtering (surface damage of FeS₂ crystals) that disfigure the XPS spectra, only spectra of unsputtered pyrite samples were used for fitting the spectra to the spectral components.

The Fe 2p XPS spectra (in Fig. 5a, c, e, g) include contributions from bulk Fe²⁺ 2p_{3/2} emission near 707 eV [10,35], which is the most characteristic to the pyrite phase. The peak at 707 eV is more obvious for samples that were crystallized in KI flux and weaker for powders synthesized in sulphur flux. All Fe 2p spectra exhibit emissions from energies between 708 and 713.8 eV, that are attributed to the Fe³⁺ ionic

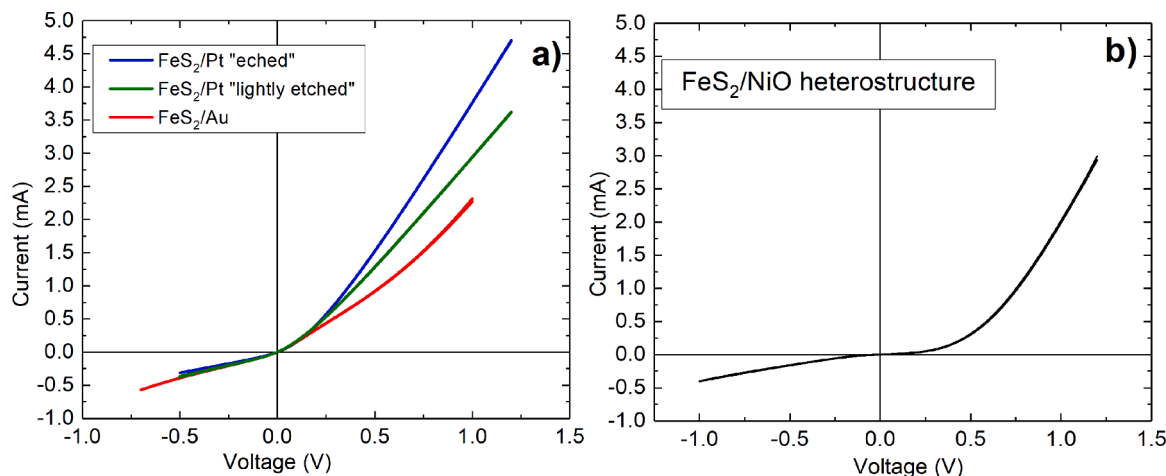


Fig. 6. *I-V* curves of FeS₂/NiO heterostructure (left) and Schottky diodes with Pt and Au contacts. Membranes with Pt electrodes were etched preliminary with “Piranha” solution (H₂SO₄: H₂O₂ = 3: 1), for 10 s in the case of “light” etching and for 60 s in the case of “etched” FeS₂ sample.

states [10,33,36]. Spectra of powders synthesized in sulphur flux have multiplet spectral contributions from FeSO₄ states at binding energies 712.2–716.6 eV [36]. Inclusion of oxygen in the samples comes likely from the impure synthesis precursors, such as elemental sulphur powder. Applied KCN etching of powders synthesized in sulphur flux did not remove any signal from SO₄²⁻ component but brought out signals of the pyrite phase (compare the Fig. 5d and Fig. 5h) by removing the intermediate (damaged by sublimation) surface layer. After the etching procedure, the Fe 2p spectre exhibits a stronger Fe²⁺ signal and clear disulphide and sulphide signals in the S 2p region. The removal of FeS and FeS_x can be described by the following reaction [37]:



The Fe 2p_{3/2} signal that appeared at 709 eV after etching the crystals with “Piranha” solution (compare Fig. 5a and Fig. 5e) is an evidence of Fe₂O₃ formation on the surface [33,38]. It indicates that some of the Fe²⁺ had been oxidized to Fe³⁺. It seems that the treatment with “Piranha” solution in the used conditions (concentration, temperature and time) did not help to avoid the phenomenon of surface Fe²⁺ oxidation to Fe³⁺ upon surface fracture (disruption of S-S bond) that was described by Nesbitt et al. [10].

The S 2p XPS spectra (in Fig. 5b, d, f, h) include bulk disulfide S₂²⁻ contributions with a doublet signal at 162.6 eV. Separation of the S 2p_{3/2} and S 2p_{1/2} doublet is 1.2 eV [10,34,38]. The S part of XPS spectrum of the powder synthesized in sulphur and sublimed (see Fig. 5d), exhibits only a very weak doublet of peaks at energies 162.9 and 164 eV attributed to elemental sulphur in the Ref. [34]. This is a suggestion that the used vacuum sublimation removed almost all of the sulphur from the utmost surface of FeS₂ crystals. The XPS spectrum recorded after following KCN etching (Fig. 5h) revealed again the disulfide S₂²⁻ contributions that belong to the pyrite phase. This fact suggests that applying KCN etching to the sublimed powder reveals the pyrite surface (compare Fig. 5d and Fig. 5h) by dissolving and removing surface FeS_x into etching solution via complexing Fe into hexacyanoferrate complex ions (reaction 1). Doublet peaks of elemental sulphur S⁰ and polysulphide S₈⁻ at 163.5 and 164.7 eV and at 164.6 and 165.8 eV, respectively, are apparent in Fig. 5h. In Ref. [10,34] these doublets were attributed to the unreacted elemental sulphur.

Based on XPS analysis it was concluded that a) vacuum sublimation results in sulphur-poor FeS₂ surface that can be restored by following KCN etching; b) the “Piranha” treatment in the used conditions (concentration, temperature and time) did not help to avoid the phenomenon of surface Fe²⁺ oxidation to Fe³⁺; c) the crystals synthesized in KI flux exhibited stronger indication of the pyrite phase and less secondary compounds such as FeSO₄. One reason for the formation and growth of

more developed crystals in molten KI is its lower viscosity. The diffusion dynamics for the growth of pyrite crystals is different in liquid S and KI. Sulphur has higher viscosity – 0.1 Pa·s at its boiling point, 445 °C [39], which is below the growth temperature of 500 °C; viscosity of KI is 0.0012 Pa·s at 740 °C [40]. The lower viscosity helps to dissolve and diffuse the material through liquid flux, therefore the larger crystals grow.

3.5. Schottky diodes and FeS₂/NiO hetero structure

The FeS₂ powder recrystallized in KI was sieved into narrow size fractions and the unisize crystals were used for the monograin membrane formation in order to prepare Schottky diodes and FeS₂/NiO heterostructure. Prior to device fabrication, the pyrite crystals surface was passivated. The surface was removed by etching with “Piranha” solution (H₂SO₄: H₂O₂ = 3:1), which is an oxidizing etchant that has been used by researchers [11,41] for improving pyrite surface parameters. Etching time was 10 s in the case of “light etching”, which was done for the pyrite membranes on epoxy. 60 s etching regime was done for pyrite microcrystals prior to MGL fabrication. After etching procedures, the powders and membranes were cleaned with water and used for device fabrication.

It was detected by hot probe measurements, that pyrite microcrystals exhibited *n*-type conductivity. Thus, the finding of a suitable metal with higher work function than that of pyrite was needed. FeS₂ has work function of 3.9 eV [42], meaning that the work function of a partnering metal should be higher. Pt and Au with work functions of 6.1 eV and 5.45 eV, respectively [43,44], were deposited on pyrite monolayer membranes as *p/n* junction partners for pyrite/Pt and Pyrite/Au Schottky diodes. The current-voltage (*I-V*) curve of the formed diodes can be seen in Fig. 6a.

P-type NiO was deposited by SILAR method to form heterostructure with the pyrite membrane. *I-V* curve of heterostructure can be seen on Fig. 6b, unfortunately it didn't generate current and indicated the existence of pinholes in the structure. Charge carriers' concentrations 6.2 × 10¹⁶ and 2.5 × 10¹⁷ cm⁻³ were found from *C-V* measurements using FeS₂/NiO heterostructures and FeS₂/Pt Schottky diodes, respectively. These values are in good agreement with the results reported in literature [45].

4. Conclusion

In the current work we developed a procedure for growth of pyrite microcrystals to be used in monograin layer solar cell. FeS₂ microcrystals synthesized in sulphur and recrystallized in molten KI as flux, had

cubic structure of pyrite phase with stoichiometric composition, as confirmed by XRD, Raman and EDX analyses, respectively. Based on XPS analysis it was concluded that a) vacuum sublimation results in sulphur-poor FeS₂ surface that can be restored by following KCN etching; b) the “Piranha” treatment in the used conditions (concentration, temperature and time) did not help to avoid the phenomenon of surface Fe²⁺ oxidation to Fe³⁺; c) the crystals synthesized in KI flux exhibited stronger indication of the pyrite phase and less secondary compounds such as FeSO₄. Grown crystals exhibited *n*-type conductivity determined by hot probe measurements. Therefore, *p*-type NiO was deposited by the SILAR method on the top of the crystals in order to form FeS₂/NiO heterostructure. Additionally, FeS₂ Schottky diodes were fabricated with Pt and Au contacts. Via the *C*-*V* measurements, the charge carriers' concentrations of 6.2×10^{16} and 2.5×10^{17} cm⁻³ were found using FeS₂/NiO heterostructures and FeS₂/Pt Schottky diodes, respectively.

CRedit authorship contribution statement

Katriin Kristmann: Writing – original draft, Writing – review & editing, Investigation, Formal analysis. **Mare Altsaar:** Writing – review & editing, Formal analysis. **Jaan Raudoja:** Resources. **Jüri Krustok:** Writing – original draft, Investigation. **Maris Pilvet:** Resources. **Valdek Mikli:** Investigation, Formal analysis. **Maarja Grossberg:** Writing – original draft, Supervision, Funding acquisition, Project administration. **Mati Danilson:** Investigation, Writing – review & editing, Formal analysis. **Taavi Raadik:** Writing – original draft, Writing – review & editing, Investigation, Funding acquisition, Project administration.

Declaration of Competing Interest

The authors declare the following financial interests/personal relationships which may be considered as potential competing interests

Acknowledgement

This work has been supported by the European Regional Development Fund, Project TK141, Estonian Research Council project PRG1023, ERDF project "Center of nanomaterials technologies and research (NAMUR+)" (2014–2020.4.01.16–0123), Mobilitas Plus Returning Researcher Grant MOBTP131 and ESA Discovery programme under Contract no. 4000134676.

References

- [1] A. Le Donne, V. Trifiletti, S. Binetti, New earth-abundant thin film solar cells based on chalcogenides, *Front. Chem.* 7 (2019), <https://doi.org/10.3389/fchem.2019.00297>.
- [2] L. Yu, S. Lany, R. Kykyneshi, V. Jieratum, R. Ravichandran, B. Pelatt, E. Altschul, H.A.S. Platt, J.F. Wager, D.A. Keszler, A. Zunger, Iron chalcogenide photovoltaic absorbers, *Adv. Energy Mater.* (2011), <https://doi.org/10.1002/aenm.201100351>.
- [3] M. Rahman, G. Boschloo, A. Hagfeldt, T. Edvinsson, On the mechanistic understanding of photovoltage loss in iron pyrite solar cells, *Adv. Mater.* (2020), <https://doi.org/10.1002/adma.201905653>.
- [4] C. Steinhagen, T.B. Harvey, C.J. Stolle, J. Harris, B.A. Korgel, Pyrite nanocrystal solar cells: promising, or fool's gold? *J. Phys. Chem. Lett.* (2012) <https://doi.org/10.1021/jz301023c>.
- [5] R.P. Srivastava, A.P. Saxena, S. Ingole, *n*-Type iron pyrite (FeS₂) thin-films obtained at different sulfur vapor pressures, *Chalcogenide Lett* (2017).
- [6] C. Wadia, A.P. Alivisatos, D.M. Kammen, Materials availability expands the opportunity for large-scale photovoltaics deployment, *Environ. Sci. Technol.* (2009), <https://doi.org/10.1021/es8019534>.
- [7] A. Ennaoui, H. Tributsch, Iron sulphide solar cells, *Sol. Cells.* (1984), [https://doi.org/10.1016/0379-6787\(84\)90009-7](https://doi.org/10.1016/0379-6787(84)90009-7).
- [8] K. Ellmer, C. Hopfner, On the stoichiometry of the semiconductor pyrite (FeS₂), *Philos. Mag. A Phys. Condens. Matter, Struct. Defects Mech. Prop.* (1997), <https://doi.org/10.1080/01418619708214015>.
- [9] M. Limpinsel, N. Farhi, N. Berry, J. Lindemuth, C.L. Perkins, Q. Lin, M. Law, An inversion layer at the surface of *n*-type iron pyrite, *Energy Environ. Sci.* (2014), <https://doi.org/10.1039/c3ee43169j>.
- [10] H.W. Nesbitt, Sulfur and iron surface states on fractured pyrite surfaces, *Am. Mineral.* (1998), <https://doi.org/10.2138/am-1998-9-1015>.
- [11] J. Walter, X. Zhang, B. Voigt, R. Hool, M. Manno, F. Mork, E.S. Aydil, C. Leighton, Surface conduction in *n*-type pyrite FeS₂ single crystals, *Phys. Rev. Mater.* (2017), <https://doi.org/10.1103/PhysRevMaterials.1.065403>.
- [12] M. Altsaar, A. Jagomägi, M. Kauk, M. Krunks, J. Krustok, E. Mellikov, J. Raudoja, T. Varema, Monograin layer solar cells, *Thin Solid Films* (2003), [https://doi.org/10.1016/S0040-6090\(03\)00167-6](https://doi.org/10.1016/S0040-6090(03)00167-6).
- [13] K. Timmo, M. Kauk-Kuusik, M. Pilvet, M. Altsaar, M. Grossberg, M. Danilson, R. Kaupmees, V. Mikli, J. Raudoja, T. Varema, Cu(In,Ga)Se₂ monograin powders with different Ga content for solar cells, *Sol. Energy.* 176 (2018) 648–655, <https://doi.org/10.1016/j.solener.2018.10.078>.
- [14] O. Kubaschewski von Goldbeck, Iron–sulphur Fe–S. IRON–Binary Phase Diagrams, Springer-Verlag, 1982, pp. 125–128, <https://doi.org/10.1007/978-3-662-08024-5>.
- [15] D. Shishin, E. Jak, S.A. Decterov, Critical assessment and thermodynamic modeling of the Fe–O–S system, *J. Phase Equilibria Diffus.* (2015), <https://doi.org/10.1007/s11669-015-0376-4>.
- [16] M. Altsaar, E. Mellikov, CuInSe₂ monograin growth in CuSe–Se liquid phase, *Jpn. J. Appl. Phys.* (2000), <https://doi.org/10.7567/jjaps.39s1.65>.
- [17] Y.-H. Chen, Y.-H. Chen, W.-D. Hsu, Y.-C. Chang, H.-S. Sheu, J.-J. Lee, S.-K. Lin, Using the high-temperature phase transition of iron sulfide minerals as an indicator of fault slip temperature, *Sci. Rep.* 9 (2019), <https://doi.org/10.1038/s41598-019-44319-8>.
- [18] W.M. Haynes, *CRC Handbook of Chemistry and Physics, Internet Version, 95th Edition*, CRC Press/Taylor and Francis, Boca Raton, FL, 2015.
- [19] Y. Akaltun, T. Çayır, Fabrication and characterization of NiO thin films prepared by SILAR method, *J. Alloys Compd.* (2015) 625, <https://doi.org/10.1016/j.jallcom.2014.10.194>.
- [20] I. Leinemann, K. Timmo, M. Grossberg, T. Kaljuvee, K. Tõnsuaadu, R. Traksmaa, M. Altsaar, D. Meissner, Reaction enthalpies of Cu₂ZnSnSe₄ synthesis in KI, *J. Therm. Anal. Calorim.* (2015), <https://doi.org/10.1007/s10973-014-4339-5>.
- [21] K. Timmo, M. Kauk-Kuusik, M. Pilvet, M. Altsaar, M. Grossberg, M. Danilson, R. Kaupmees, V. Mikli, J. Raudoja, T. Varema, Cu(In,Ga)Se₂ monograin powders with different Ga content for solar cells, *Sol. Energy.* (2018), <https://doi.org/10.1016/j.solener.2018.10.078>.
- [22] M. Altsaar, J. Raudoja, K. Timmo, M. Danilson, M. Grossberg, M. Krunks, T. Varema, E. Mellikov, Cu₂ZnSnSe₄ monograin powders for solar cell application, in: *Conf. Rec. 2006 IEEE 4th World Conf. Photovolt, Energy Conversion, WCPEC-4, 2006*, <https://doi.org/10.1109/WCPEC.2006.279492>.
- [23] K. Timmo, M. Kauk-Kuusik, M. Pilvet, V. Mikli, E. Kärber, T. Raadik, I. Leinemann, M. Altsaar, J. Raudoja, Comparative study of SnS recrystallization in molten CdI₂, SnCl₂ and KI, *Phys. Status Solidi Curr. Top. Solid State Phys.* (2016), <https://doi.org/10.1002/pssc.201510082>.
- [24] H. Vogt, T. Chattopadhyay, H.J. Stolz, Complete first-order Raman spectra of the pyrite structure compounds FeS₂, MnS₂ AND SiP₂, *J. Phys. Chem. Solids.* (1983), [https://doi.org/10.1016/0022-3697\(83\)90124-5](https://doi.org/10.1016/0022-3697(83)90124-5).
- [25] A.N. Utyuzh, Influence of temperature on raman spectra of the FeS₂ single crystal with pyrite structure, *Phys. Solid State.* (2014), <https://doi.org/10.1134/S1063783414100321>.
- [26] D.L.A. De Faria, S. Venâncio Silva, M.T. De Oliveira, Raman microspectroscopy of some iron oxides and oxyhydroxides, *J. Raman Spectrosc.* 28 (1997) 876–878, [https://doi.org/10.1002/\(sici\)1097-4555\(199711\)28:11<873::aid-jrs177>3.0.co;2-b](https://doi.org/10.1002/(sici)1097-4555(199711)28:11<873::aid-jrs177>3.0.co;2-b).
- [27] A.T. Ward, Raman spectroscopy of sulfur, sulfur-selenium, and sulfur-arsenic mixtures, *J. Phys. Chem.* (1968), <https://doi.org/10.1021/j100858a031>.
- [28] Y. El Mendili, A. Abdelouas, H. El Hajj, J.-F. Bardeau, Phase transitions of iron sulphides formed by steel microbial corrosion, *RSC Adv* 3 (2013) 26343–26351, <https://doi.org/10.1039/c3ra45259j>.
- [29] M. Grossberg, J. Krustok, J. Raudoja, K. Timmo, M. Altsaar, T. Raadik, Photoluminescence and Raman study of Cu₂ZnSn(Se xS₁ - X)₄ monograin for photovoltaic applications, *Thin Solid Films* (2011), <https://doi.org/10.1016/j.tsf.2010.12.099>.
- [30] A. Zavrzhnov, A. Naumov, A. Kosyakov, S. Berezin, V. Volkov, A. Sergeeva, The Iron Sulfides Crystal Growth from the Halide Melts, *Mater. Res.* (2018), <https://doi.org/10.1590/1980-5373-mr-2017-0648>.
- [31] P. Prabukanthan, S. Thamaraiselvi, G. Harichandran, Single step electrochemical deposition of *p*-Type Undoped and Co²⁺ doped FeS₂ thin films and performance in heterojunction solid solar cells, *J. Electrochem. Soc.* (2017), <https://doi.org/10.1149/2.0991709jes>.
- [32] H. Ning, Z. Liu, Y. Xie, H. Huang, CoS₂ coatings for improving thermal stability and electrochemical performance of FeS₂ cathodes for thermal batteries, *J. Electrochem. Soc.* (2018), <https://doi.org/10.1149/2.0321809jes>.
- [33] C.M. Eggleston, J.-J. Ehrhardt, W. Stumm, Surface structural controls on pyrite oxidation kinetics; an XPS-UPS, STM, and modeling study, *Am. Mineral.* (1996) 81, <https://doi.org/10.2138/am-1996-9-1002>.
- [34] M. Fantauzzi, B. Elsener, D. Atzei, A. Rigoldi, A. Rossi, Exploiting XPS for the identification of sulfides and polysulfides, *RSC Adv* 5 (2015), <https://doi.org/10.1039/C5RA14915K>.
- [35] P. Behra, P. Bonnisel-Gissingner, M. Alnot, R. Revel, J.J. Ehrhardt, XPS and XAS Study of the Sorption of Hg(II) onto Pyrite, *Langmuir* (2001) 17, <https://doi.org/10.1021/la0014510>.
- [36] A.P. Grosvenor, B.A. Kobe, M.C. Biesinger, N.S. McIntyre, Investigation of multiple splitting of Fe 2p XPS spectra and bonding in iron compounds, *Surf. Interface Anal.* 36 (2004), <https://doi.org/10.1002/sia.1984>.
- [37] G. Senanayake, The cyanidation of silver metal: review of kinetics and reaction mechanism, *Hydrometallurgy* (2006) 81, <https://doi.org/10.1016/j.hydromet.2005.12.001>.

- [38] Z. Mutlu, B. Debnath, S. Su, C. Li, M. Ozkan, K.N. Bozhilov, R.K. Lake, C.S. Ozkan, Chemical vapor deposition and phase stability of pyrite on SiO₂, *J. Mater. Chem. C.* (2018) 6, <https://doi.org/10.1039/C8TC00584E>.
- [39] R. Steudel, Liquid sulfur, in: R. Steudel (Ed.), *Elemental Sulfur and Sulfur-Rich Compounds I*, Springer-Verlag, 2003, pp. xx–yy, <https://doi.org/10.1007/b12115>.
- [40] Y. Sato, M. Fukasawa, T. Yamamura, Viscosities of molten alkali-metal bromides and iodides, *Int. J. Thermophys.* (1997), <https://doi.org/10.1007/BF02575253>.
- [41] M. Limpinsel, *Ph.D. Thesis, University of California, Irvine, 2015*.
- [42] P.P. Altermatt, T. Kiesewetter, K. Ellmer, H. Tributsch, Specifying targets of future research in photovoltaic devices containing pyrite (FeS₂) by numerical modelling, *Sol. Energy Mater. Sol. Cells.* (2002), [https://doi.org/10.1016/S0927-0248\(01\)00053-8](https://doi.org/10.1016/S0927-0248(01)00053-8).
- [43] W.M.H. Sachtler, G.J.H. Dorgelo, A.A. Holscher, The work function of gold, *Surf. Sci.* (1966), [https://doi.org/10.1016/0039-6028\(66\)90083-5](https://doi.org/10.1016/0039-6028(66)90083-5).
- [44] G.N. Derry, Z. Ji-Zhong, Work function of Pt(111), *Phys. Rev. B.* (1989), <https://doi.org/10.1103/PhysRevB.39.1940>.
- [45] G. Willeke, O. Blenk, C. Kloc, E. Bucher, Preparation and electrical transport properties of pyrite (FeS₂) single crystals, *J. Alloys Compd.* (1992), [https://doi.org/10.1016/0925-8388\(92\)90260-G](https://doi.org/10.1016/0925-8388(92)90260-G).